AFRL-AFOSR-VA-TR-2023-0240

Studies of Finite-Rate Effects Relevant to Modeling of Liquid-Propellant Rocket Combustion Instabilities

Sanchez, Antonio
UNIVERSITY OF CALIFORNIA, SAN DIEGO
9500 GILMAN DR
LA JOLLA, CA, 92093
USA

01/04/2023
Final Technical Report

DISTRIBUTION A: Distribution approved for public release.

Air Force Research Laboratory
Air Force Office of Scientific Research
Arlington, Virginia 22203
Air Force Materiel Command

REPORT DOCUMENTATION PAGE

PLEASE DO NOT RETURN YOUR FORM TO THE ABOVE ORGANIZATION.

1. REPORT DATE	2. REPORT TYPE	3. DATES COVERED	
20230104	Final	START DATE 20200930	END DATE 20220929

4. TITLE AND SUBTITLE
Studies of Finite-Rate Effects Relevant to Modeling of Liquid-Propellant Rocket Combustion Instabilities

5a. CONTRACT NUMBER	5b. GRANT NUMBER	5c. PROGRAM ELEMENT NUMBER
	FA9550-20-1-0431	61102F
5d. PROJECT NUMBER	**5e. TASK NUMBER**	**5f. WORK UNIT NUMBER**

6. AUTHOR(S)
Antonio Sanchez

7. PERFORMING ORGANIZATION NAME(S) AND ADDRESS(ES)
UNIVERSITY OF CALIFORNIA, SAN DIEGO
9500 GILMAN DR
LA JOLLA, CA 92093
USA

8. PERFORMING ORGANIZATION REPORT NUMBER

9. SPONSORING/MONITORING AGENCY NAME(S) AND ADDRESS(ES)	10. SPONSOR/MONITOR'S ACRONYM(S)	11. SPONSOR/MONITOR'S REPORT NUMBER(S)
Air Force Office of Scientific Research 875 N. Randolph St. Room 3112 Arlington, VA 22203	AFRL/AFOSR RTA1	AFRL-AFOSR-VA-TR-2023-0240

12. DISTRIBUTION/AVAILABILITY STATEMENT
A Distribution Unlimited: PB Public Release

13. SUPPLEMENTARY NOTES

14. ABSTRACT
The goal of this project is to advance fundamental knowledge pertaining to the interplay of the acoustic ï¬•eld with the reactive ï¬‚ow in liquid-propellant rocket engines, enabling the development of advanced modeling tools for predicting the instability behavior in realistic scenarios. Our work combines numerical and modeling eï¬€orts in linear and nonlinear studies of unsteady ï¬‚ames, with a focus on the development and application of quasi-steady-state reduced-chemistry mechanisms to the development of submodels for the numerical computation of liquid-propellant rocket instabilities. Speciï¬•c objectives include the generation and validation of advanced ï¬‚amelet models for future use in improved LES calculations of acoustic combustion instabilities and the investigation of ï¬‚ame dynamics in the near-injector region, with the latter investigation speciï¬•cally addressing propagation of partially premixed fronts along mixing layers.

15. SUBJECT TERMS

16. SECURITY CLASSIFICATION OF:			17. LIMITATION OF ABSTRACT	18. NUMBER OF PAGES
a. REPORT U	b. ABSTRACT U	c. THIS PAGE U	UU	22

19a. NAME OF RESPONSIBLE PERSON	19b. PHONE NUMBER *(Include area code)*
MITAT BIRKAN	426-7234

Studies of Finite-Rate Effects Relevant to Modeling of Liquid-Propellant Rocket Combustion Instabilities.

Antonio L. Sánchez (PI), Forman A. Williams,
Department of Mechanical and Aerospace Engineering
University of California, San Diego

Department: **Space Power and Propulsion**
Program Officer: **Dr. Mitat A. Birkan**

1 Accomplishments

1.1 Research Objectives

The goal of this project is to advance fundamental knowledge pertaining to the interplay of the acoustic field with the reactive flow in liquid-propellant rocket engines, enabling the development of advanced modeling tools for predicting the instability behavior in realistic scenarios. Our work combines numerical and modeling efforts in linear and nonlinear studies of unsteady flames, with a focus on the development and application of quasi-steady-state reduced-chemistry mechanisms to the development of submodels for the numerical computation of liquid-propellant rocket instabilities. Specific objectives include the generation and validation of advanced flamelet models for future use in improved LES calculations of acoustic combustion instabilities and the investigation of flame dynamics in the near-injector region, with the latter investigation specifically addressing propagation of partially premixed fronts along mixing layers.

1.2 Detailed description of specific accomplishments

1.2.1 Systematically derived one-step kinetics for hydrogen combustion at elevated pressures

There is continuing interest in developing methods for computationally predicting flame dynamics, including combustion instabilities, in liquid-propellant rockets and other engines (LPREs). Because of the excessive computer time required in computations involving detailed chemistry, there is interest in introducing simplified chemistry descriptions to facilitate and speed up the simulations. Simplifications to the detailed chemistry follow from application of systematic reduction techniques aimed at lowering the order and complexity of the system of differential conservation equations to be integrated by reducing the effective number of chemical species and chemical reactions to be considered in the simulation [1, 2]. The complex interactions between the chemistry, the flow, and the acoustic field can be examined effectively on the basis of reduced chemical-kinetic mechanisms systematically derived from detailed chemical schemes by introduction of steady states for intermediate species [3]. The resulting reduced mechanisms, comprising a short number of overall reactions among a few chemical species, are more appropriate both for implementation in commercial codes and for enabling the development of fundamental physical understanding.

Our recent efforts to derive and test reduced kinetic descriptions have focused on high-pressure conditions and unsteady flame response, not specifically addressed in previous studies. Although hydrogen is used as target fuel, many of the conclusions are expected to be applicable to hydrocarbon systems. Hydrogen is widely used in LPREs. Also, because of their environmental and economic benefits, hydrogen-fueled gas turbines are bound to play an important role in foreseeable carbon-free energy-production scenarios [4]. Manufactures are moving from systems fueled by natural gas to new designs involving hydrogen addition to carbon-containing or carbon-free fuels, such as ammonia, or simply using only hydrogen. Experimental and computational investigations have shown, however, that hydrogen affects gas-turbine combustion processes substantially [5]. A critical need therefore exists for simple and efficient means for describing the chemical kinetics of hydrogen combustion sufficiently accurately under rocket and gas-turbine conditions.

Different approaches have been pursued in deriving simplified kinetics for hydrogen combustion. A single overall step has been derived on the basis of detailed-chemistry flame computations by selecting the Arrhenius rate parameters from a least square fit of the heat release profile [6]. Similar one-step descriptions targeting specific combustion conditions have been shown to be useful in addressing particular problems, including deflagration-to-detonation transition [7] and supersonic combustion [8]. The accuracy of all of these ad hoc descriptions degrades rapidly outside the narrow ranges of temperature, pressure, and composition for which they were originally developed, so that their utility is limited. Reduced mechanisms that are systematically derived from first principles are more useful in that respect. Simplifications can be achieved through introduction of steady-state approximations for chemical intermediates that exhibit negligibly small transport rates, resulting in reduced mechanisms involving a few overall steps with global reaction rates that are evaluated from those of the elementary reactions [9]. For example, for hydrogen a two-step mechanism with H as the only intermediate not following steady state has been shown to describe with sufficient accuracy flame propagation under a wide range of conditions [10]. More complicated descriptions apply in autoignition processes, for which either HO_2 (above the second explosion limit) or H_2O_2 (below the second explosion limit) are found to be out of steady state [11]. The steady-state assumption for OH loses accuracy when autoignition takes place in nonpremixed environments, including laminar mixing layers [12] and turbulent jets [13], for which a minimum of three global steps are needed. Following these previous ideas, the current investigation exploits steady-state simplifications applying for hydrogen-air and hydrogen-oxygen combustion at high pressure, under which conditions a one-step mechanism suffices to describe many aspects of the combustion process, as explained below.

The high-pressure conditions prevailing in rocket combustion chambers and gas-turbine combustors promote radical recombination through three-body recombination reactions in such a way that the rate of radical branching and that of radical recombination do not differ by a large amount in the thin hot reaction layers where the fuel is oxidized, so that the key intermediates H, O, OH, and HO_2 maintain steady states there, their transport rates playing minor roles in determining the local heat-release rate. Under those conditions, hydrogen oxidation effectively proceeds according to the global reaction

$$2H_2 + O_2 \rightarrow 2H_2O, \tag{1}$$

with an overall rate that can be expressed in closed analytic form in terms of the local temperature and the O_2, H_2, and H_2O concentrations [14], thereby providing an attractive simple chemistry description. The level of accuracy to be expected when using this one-step chemistry in rocket and gas-turbine combustion simulations is to be assessed below through flamelet computations involving three canonical configurations, namely, steady planar deflagrations, counterflow premixed and nonpremixed flames, and two-dimensional triple flames.

Description of the one-step chemistry For the combustion conditions typically found in rocket engines and gas turbines, hydrogen oxidation is controlled by nine elementary steps [9], namely, the reversible shuffle reactions $H+O_2 \overset{1}{\rightleftharpoons} OH+O$, $H_2+O \overset{2}{\rightleftharpoons} OH+H$, and $H_2+OH \overset{3}{\rightleftharpoons} H_2O+H$, the irreversible three-body reactions $H+O_2+M \overset{4f}{\rightarrow} HO_2+M$, $H+OH+M \overset{8f}{\rightarrow} H_2O+M$ and $H+H+M \overset{9f}{\rightarrow} H_2+M$, and the irreversible hydroperoxyl-consumption reactions $HO_2+H \overset{5f}{\rightarrow} OH+OH$, $HO_2+H \overset{6f}{\rightarrow} H_2+O_2$, and $HO_2+OH \overset{7f}{\rightarrow} H_2O+O_2$. Corresponding reaction-rate constants k can be found in [15], including separate expressions for the rate parameters of the forward (f) and backward (b) reactions.

As shown in [14], when all hydrogen-oxygen radicals obey a steady-state approximation, the combined effect of all nine elementary reactions can be represented by the global reaction (1) whose rate ω (moles per unit volume per unit time) is given by the sum of the elementary rates of reactions $4f$, $8f$, and $9f$, thereby giving

$$\omega = k_{4f} C_{\mathrm{M}_4} C_{\mathrm{O}_2} C_{\mathrm{H}} + k_{8f} C_{\mathrm{M}_8} C_{\mathrm{OH}} C_{\mathrm{H}} + k_{9f} C_{\mathrm{M}_9} C_{\mathrm{H}}^2, \tag{2}$$

where C_i and C_{M_j} denote the concentration of species i and the effective third-body concentration, the latter evaluated for each reaction $j = (4f, 8f, 9f)$ with account taken of its specific chaperon efficiencies. The rate (2) depends on the local values of the H and OH concentrations, which can be determined by algebraic manipulation of the steady-state equations for H, OH, O, and HO_2 to yield [14]

$$C_{\mathrm{H}} = \frac{1}{GH} \frac{k_{2f} k_{3f} C_{\mathrm{H}_2}^2}{k_{1b} k_{4f} C_{\mathrm{M}_4} C_{\mathrm{O}_2}} \left(\frac{k_{1f}}{\alpha k_{4f} C_{\mathrm{M}_4}} - 1 \right), \tag{3}$$

and

$$C_{\mathrm{OH}} = \frac{1}{H} \frac{k_{2f} C_{\mathrm{H}_2}}{k_{1b}} \left(\frac{k_{1f}}{\alpha k_{4f} C_{\mathrm{M}_4}} - 1 \right), \tag{4}$$

involving the three dimensionless functions G, H, and

$$\alpha = \frac{k_{6f} f/(k_{5f} + k_{6f}) + G}{f + G}, \tag{5}$$

with

$$f = \frac{k_{5f} + k_{6f}}{k_{7f}} \frac{k_{3f}}{k_{4f} C_{\mathrm{M}_4}} \frac{C_{\mathrm{H}_2}}{C_{\mathrm{O}_2}} \tag{6}$$

(expressions for the order-unity functions G and H are considerably more involved and can be found in [14]). The resulting overall rate depends on the temperature and on the concentrations of H_2, O_2, and H_2O, the last dependence entering in the function G through the backward reaction $H_2O+H \overset{3b}{\rightarrow} H_2+OH$ [14]. Although almost impossibly complex algebraically, it is exceedingly simple computationally to evaluate ω directly from (2).

As can be seen from the formulas above, the radical concentrations (3) and (4) contain a cutoff factor $(k_{1f} - \alpha k_{4f} C_{\mathrm{M}_4})$ that becomes zero as the temperature T reaches the crossover value T_c at which the rate of radical production matches the rate of radical recombination, as defined by the condition

$$k_{1f} = \alpha k_{4f} C_{\mathrm{M}_4}. \tag{7}$$

In the present approximation, all radical concentrations vanish for $T < T_c$ and, correspondingly, the reaction rate (2) must be set equal to zero. Because of its key role in hydrogen combustion, it is of interest to review briefly the dependence of T_c on the combustion conditions. Besides the well-known increase with increasing pressure p, resulting from the linear proportionality $C_{\mathrm{M}_4} \propto p$, the crossover temperature determined from (7) exhibits a dependence on the mixture composition, partly because H_2 and H_2O have increased chaperon efficiencies (i.e. 16 for H_2O and 2.5 for H_2 in reaction $4f$) compared with nitrogen and other species and partly through the factor α defined in (5).

To understand the latter dependence, which enters mainly through the function f defined in (6), it is important to note that the three-body reaction $H+O_2+M \overset{4f}{\rightarrow} HO_2+M$ is chain-carrying, in that in eliminating one hydrogen atom it creates one hydroperoxyl radical, so that the total number of radicals is not altered. To determine the net recombination efficiency of reaction $4f$ one must therefore investigate the subsequent consumption of HO_2 through collisions with H and OH radicals. In very lean mixtures the prevailing consumption route involves collisions with OH through reaction $HO_2+OH \overset{7f}{\rightarrow} H_2O+O_2$, which is chain-terminating, resulting in a value of $\alpha = 1$, as can be seen by taking the limit $f \ll 1$ in (5). The associated overall rate takes in the case the simplified form

$$\omega = \left(\frac{k_{1f}}{k_{4f} C_{\mathrm{M}_4}} - 1 \right) \frac{k_{2f} k_{3f}/k_{1b}}{1 + \frac{k_{3b} C_{\mathrm{H_2O}}}{k_{4f} C_{\mathrm{M}_4} C_{\mathrm{O}_2}}} C_{\mathrm{H}_2}^2 \tag{8}$$

with the crossover temperature, determined with $\alpha = 1$ from $k_{1f} = k_{4f} C_{\mathrm{M}_4}$, taking the values $T_c \simeq 1000$ K at $p = 1$ atm and $T_c \simeq 1800$ K at $p = 40$ atm.

By way of contrast, in very rich mixtures, corresponding to the opposite limit $f \gg 1$, the concentration of H is much larger than that of OH, with the result that HO_2 consumption occurs instead through reactions $HO_2+H \overset{5f}{\rightarrow} OH+OH$ (chain-carrying) and $HO_2+H \overset{6f}{\rightarrow} H_2+O_2$ (chain-terminating). Since $k_{6f}/(k_{5f} + k_{6f}) \simeq 1/6$ regardless of the temperature, it turns out from (5) that only one sixth of the collisions involving HO_2 effectively removes radicals, a fact clearly reflected in the limiting value $\alpha \simeq k_{6f}/(k_{5f} + k_{6f}) \simeq 1/6$ of α for $f \gg 1$. Since the effective rate of radical removal through $H+O_2+M \overset{4f}{\rightarrow} HO_2+M$ is diminished, the resulting crossover temperature is significantly lower, as can be seen by evaluating $k_{1f} = (1/6) k_{4f} C_{\mathrm{M}_4}$ to give $T_c \simeq 700$ K at $p = 1$ atm and $T_c \simeq 1300$ K at $p = 40$ atm. It then can be seen by using (3) in the dominant leading term in (2) that in this limiting case the overall rate takes the simplified form

$$\omega = \left(\frac{k_{1f}}{k_{4f} C_{\mathrm{M}_4}} - \frac{k_{6f}}{k_{5f} + k_{6f}} \right) \frac{(k_{4f} C_{\mathrm{M}_4})^2}{\frac{k_{3b} C_{\mathrm{H_2O}}}{k_{3f} C_{\mathrm{H}_2}} k_{8f} C_{\mathrm{M}_8} + k_{9f} C_{\mathrm{M}_9}} C_{\mathrm{O}_2}^2, \tag{9}$$

to be used below in addressing pulsating flame dynamics as an illustrative example of the predictive capabilities of the one-step mechanism under unsteady conditions.

It can be expected that the steady-state approximation holds under conditions such that the temperature difference $T_{max} - T_c$ is limited to a few hundred kelvin, so that the resulting radical transport rate (the difference between the

production rate by radical branching and the consumption rate by radical recombination) remains significantly smaller than the chemical rates. This condition is satisfied near the lean flammability limit [17,18], as well as for sufficiently rich mixtures, with the mechanism describing accurately the dynamics of pulsating flames [16]. In general, radical steady states are favored by low values of the peak temperatures, as occurs when the mixture is diluted with combustion products, or by high values of the crossover temperature, as occurs at high pressure. The computations of high-pressure flamelets shown below, including freely propagating deflagrations, counterflow premixed and nonpremixed flames and triple flames propagating in strained mixing layers, suggest that the steady-state approximation is sufficiently accurate under conditions of interest for rocket and gas-turbine combustion, for which the simple one-step chemistry described above becomes applicable. To test the accuracy of the one-step mechanism, results are compared below with detailed-chemistry computations using the 20-step San Diego mechanism [19].

To test the accuracy of the one-step mechanism, results of different flamelet configurations involving H_2-O_2-N_2 mixtures are compared with detailed-chemistry computations using the 20-step San Diego mechanism [19] in Figs. 2-6. We begin by investigating steady planar deflagrations, first reviewing the dependence of the accuracies of flame-structure approximations on pressure.

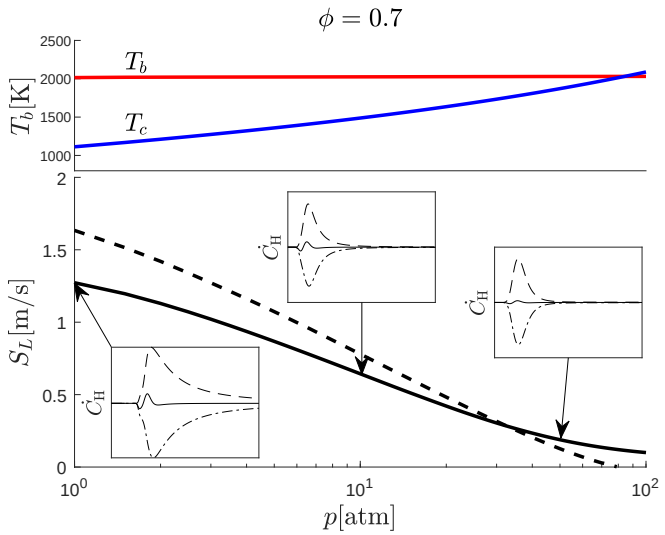

Figure 1: The variation with pressure of the burning rate S_L corresponding to lean H_2-air mixtures with equivalence ratio $\phi = 0.7$ and initial temperature $T_u = 300$ K as obtained with detailed chemistry (solid curve) and with the one-step reduced mechanism (dashed curve), with the insets showing the variation of the rates of production, consumption, and transport across the flame for three different pressures $p = (1, 10, 50)$ atm. The upper plot represents the variation of the adiabatic flame temperature T_b and of the crossover temperature T_c, the latter evaluated from (7).

Steady planar deflagrations Figure 1 shows the variation with pressure of the flame propagation velocity S_L for a lean H_2-air mixture with equivalence ratio $\phi = 0.7$ and initial temperature $T_u = 300$ K as obtained with detailed chemistry (solid curve) and reduced chemistry (dashed curve). For illustrative purposes, the equivalence ratio here was selected to lie in the vicinity of the values most often encountered in practice, the initial temperature approximating normal room temperature, but the general conclusions to be drawn concerning pressure dependences apply at essentially all conditions. The accompanying upper panel shows the variation of the corresponding adiabatic flame temperature T_b and crossover temperature T_c, the latter determined from (7) using the equilibrium composition. The computations employ a multicomponent transport description including thermal diffusion [20, 21].

To investigate the applicability of the steady-state assumption, the figure includes insets showing the rates of H-atom production, consumption and transport across the flame for three selected pressures, with the flame propagating leftward. For $p = 1$ atm, the H-atom transport rate is seen to be comparable to its production and consumption rates at the onset of reaction near the left boundary, indicating that a steady-state assumption for H atoms is inaccurate for these conditions. The relative magnitude of the transport rate diminishes as the crossover temperature approaches

the adiabatic flame temperature for increasing pressure, as can be seen in the plots for $p = 10$ atm and $p = 50$ atm. The results indicate that the steady-state approximation becomes reasonably accurate for all radicals at these intermediate high pressures 10 atm $< p <$ 50 atm, typical of gas-turbine combustion, with the consequence that the one-step reduced kinetics, which does not perform well at ambient pressure, provides a good description of the resulting burning rate, as seen in the figure. The flame velocity computed with the one-step mechanism vanishes as T_c approaches T_b, in this case for $p \simeq 80$ atm, as expected from (3) and (4). At these high pressures, radical regeneration by the hydrogen peroxide decomposition reaction H_2O_2+M $\rightarrow$ OH+OH+M opens up an alternative chain-branching path that enables fuel oxidation to proceed at a very low rate. Since the starting nine-step skeletal mechanism used in our development does not include hydrogen peroxide, these slow flames, of limited interest for practical purposes in combustion applications, cannot be described with the one-step mechanism.

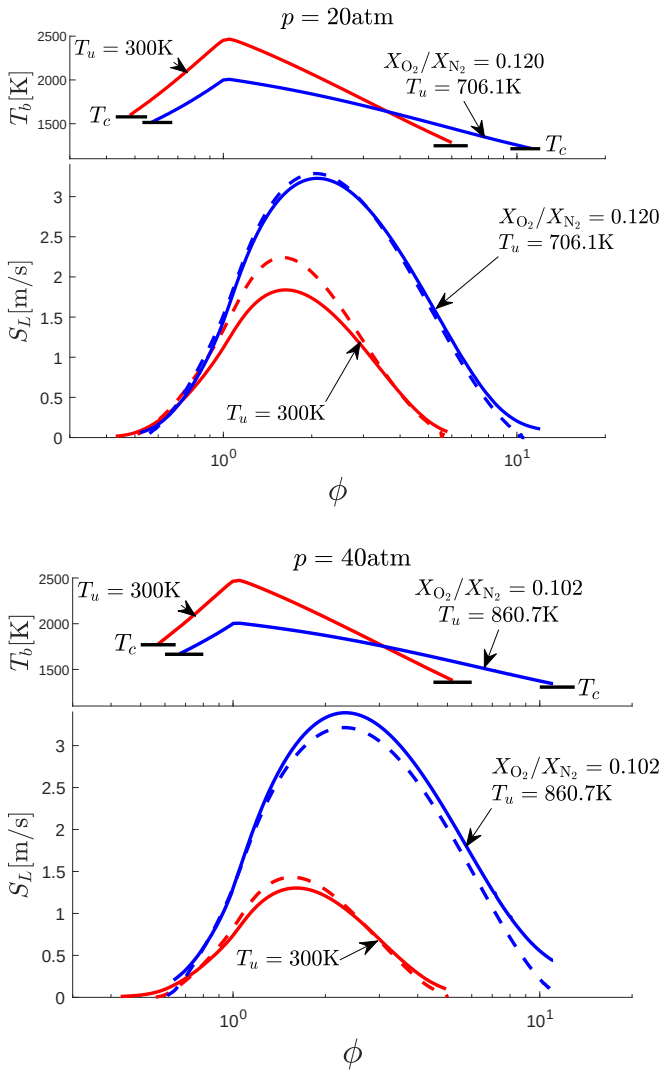

Figure 2: The variation with equivalence ratio of the burning rate S_L corresponding to H_2-air mixtures with initial temperature $T_u = 300$ K (red curves) and to preheated H_2-O_2-N_2 mixtures (blue curves) with oxygen-nitrogen mole-fraction ratio $X_{O_2}/X_{N_2} = 0.120$ ($p = 20$ atm) and $X_{O_2}/X_{N_2} = 0.102$ ($p = 40$ atm) as obtained with detailed chemistry (solid curve) and with the one-step reduced mechanism (dashed curve). The plots also include the associated variation of the adiabatic flame temperature T_b, with indication of the crossover temperature T_c corresponding to the lean and rich limits for each case.

Figure 2 shows the variation with equivalence ratio ϕ of the corresponding flame propagation velocity S_L at two different pressures. The figure also displays the variation with ϕ of the adiabatic flame temperature T_b, which is the peak temperature across the flame in the absence of heat losses, along with an indication of the corresponding crossover temperature T_c determined from the condition (7) for $\alpha = 1$ (lean limit) and $\alpha = 1/6$ (rich limit), with the chaperon efficiencies computed with the composition at equilibrium. Besides results corresponding to hydrogen-air mixtures with initial temperature $T_u = 300$ K, represented by red curves, consideration is given to preheated mixtures, with the initial temperature computed from the isentropic compression relation $T_u = 300p^{(\gamma-1)/\gamma}$ using $\gamma = 1.4$ for the specific-heat ratio, with T_u and p expressed in kelvin and atmospheres, respectively, yielding $T_u = 706.1$ K for $p = 20$ atm and $T_u = 860.7$ K for $p = 40$ atm. To represent the effect of exhaust-gas recirculation, needed to limit the peak temperature in these preheated cases, the mixture is diluted with nitrogen, with the initial oxygen-to-nitrogen mole-fraction ratio X_{O_2}/X_{N_2} lowered from the value $(X_{O_2}/X_{N_2})_{AIR} = 0.266$ corresponding to air to give an adiabatic flame temperature $T_b = 2000$ K for $\phi = 1$. The resulting values, $X_{O_2}/X_{N_2} = 0.120$ for $p = 20$ atm and $X_{O_2}/X_{N_2} = 0.102$ for $p = 40$ atm, are then used together with $\phi = 2X_{H_2}/X_{O_2}$ to determine the initial composition for the computations represented by the blue curves in Fig. 2.

The results in Fig. 2 reveal that the one-step kinetics predicts with reasonable accuracy the burning rate for all conditions explored in the figure, including mixtures where the peak temperature departs significantly from T_c. The observed relative differences in flame-propagation velocities determined with the reduced and detailed chemistries $(S_{L_{RED}} - S_{L_{DET}})/S_{L_{DET}}$ are seen to remain below about 10% for $T_{max} - T_c \lesssim 500$ K.

As previously indicated, in the one-step approximation the flame propagation velocity vanishes when the adiabatic flame temperature T_b reaches T_c, because ω becomes zero all across the flame. Therefore, the condition $T_b = T_c$ effectively introduces lean and rich chemical-kinetic flammability limits ϕ_l and ϕ_r. Since heat losses (e.g. by radiation) are not included in the computations, the curves representing detailed-chemistry results do not show these neatly defined flammability limits. Instead, at temperatures below crossover, corresponding to equivalence ratios $\phi < \phi_l$ and $\phi > \phi_r$, reactions involving H_2O_2, which are not included in the one-step mechanism because they are largely unimportant for describing flame propagation at high temperature, enable a slow path of hydrogen oxidation [9] to be followed, although radiant heat loss would soon extinguish that chemistry. The resulting nonzero values of S_L are, in addition, too small to be of practical interest, especially beyond the lean limit (i.e. $\phi < \phi_l$), where the predicted velocity is just a few centimeters per second. The detailed chemistry predicts somewhat larger values of S_L in diluted mixtures with $\phi > \phi_r \simeq 10$. The description of flame propagation under these extremely fuel-rich conditions must account, in particular, for hydroperoxyl recombination through $H_2 + HO_2 \rightarrow H_2O_2 + H$, but the associated analysis is not pursued here because this regime is of limited interest in gas-turbine applications.

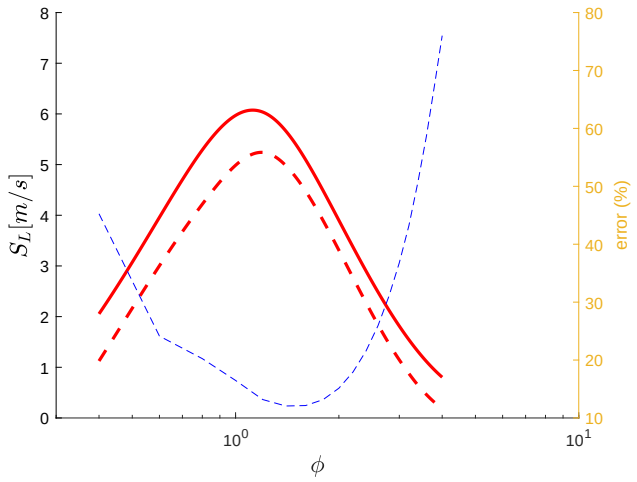

Figure 3: The variation with equivalence ratio of the burning rate S_L corresponding to H_2-O_2 mixtures with initial temperature $T_u = 200$ K and pressure $p = 300$ atm as obtained with detailed chemistry (red solid curve) and with the one-step reduced mechanism (red dashed curve), with the relative error represented with a blue thin curve.

Conditions of interest for H_2-O_2 rocket systems are investigated in Fig. 3. As can be seen, the level of accuracy of the mechanism is similar to that displayed in connection with gas-turbine combustion conditions, with errors remaining below about 20% for $0.8 < \phi < 2.0$. The results indicate that for the conditions selected, typical of LPREs, the steady state assumption for all radicals hold, despite the extreme peak temperatures prevailing in these systems. Future work should test predictive capabilities over extended ranges of pressure.

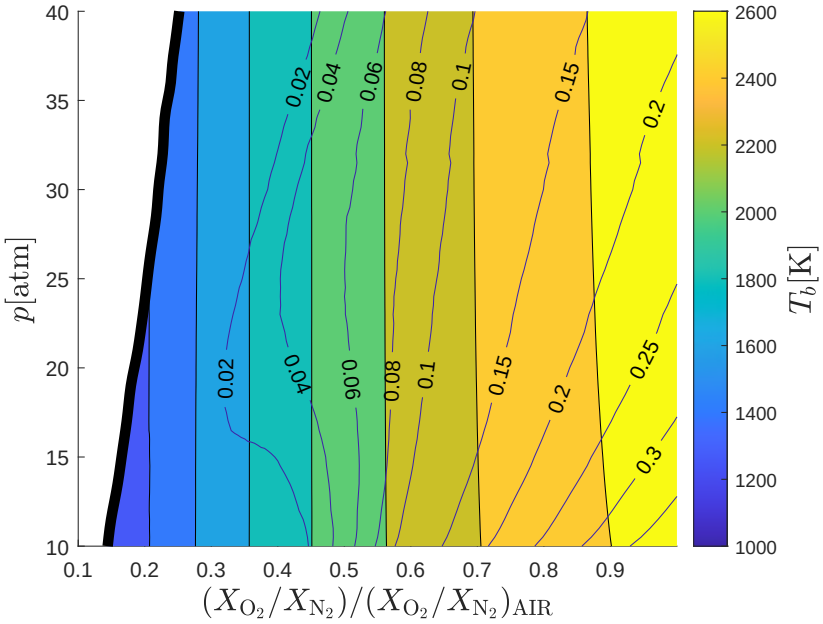

Figure 4: The variation with pressure and dilution of the relative error $(S_{L_{\rm RED}} - S_{L_{\rm DET}})/S_{L_{\rm DET}}$ in computations of stoichiometric laminar-flame propagation velocities for an initial temperature $T_u = 700$ K. Color contours are used to indicate the accompanying variation of the adiabatic flame temperature.

To further assess the accuracy of the one-step kinetics in combustion scenarios involving high-pressure diluted flames, of interest in gas-turbine combustion, additional results of flame-propagation computations pertaining to stoichiometric H_2-air mixtures diluted with nitrogen are addressed in the diagram shown in Fig. 11. The computations correspond to preheated mixtures with $T_u = 700$ K for pressures in the range 10 atm $< p <$ 40 atm. At each pressure, the mixture oxygen-to-nitrogen ratio X_{O_2}/X_{N_2} is varied from the value $(X_{O_2}/X_{N_2})_{AIR} = 0.266$ corresponding to air down to the value that yields $T_b = T_c$, beyond which the stoichiometric mixture is no longer flammable according to the one-step chemistry. Isocontours of constant relative error $(S_{L_{\rm RED}} - S_{L_{\rm DET}})/S_{L_{\rm DET}}$ are plotted along with color contours of peak temperature T_b. As can be seen, over the entire range of pressures considered in the figure, errors between about 2 % and 10 % can be expected in gas turbines operating at peak temperatures in the range 1600 K $\lesssim T_b \lesssim$ 2200 K, those being the conditions most often found in applications.

Counterflow flames The performance of the mechanism in connection with strained flamelets was investigated in computations of one-dimensional premixed and nonpremixed flames in planar counterflow mixing layers at $p = 25$ atm and $p = 50$ atm (see [22] for details of the formulation and associated simplifications). Results of twin premixed flames generated in configurations with identical opposed streams at $T = 300$ K are shown in the upper plots of Fig. 4 for H_2-O_2-N_2 mixtures with $\phi = 0.7$ and three different levels of dilution, including undiluted H_2-air mixtures (i.e. $X_{O_2}/X_{N_2} = 0.266$). These conditions were selected to correspond to those in Fig. 1. The plots represent the variation of the peak temperature over a wide range of strain rates A extending over about two orders of magnitude up to extinction. The curves show the expected superadiabatic temperatures at intermediate values of the strain rate, a result attributable to effects of preferential diffusion of hydrogen [23]. For H_2-air mixtures, the performance of the one-step mechanism is not satisfactory, especially near extinction, as may be seen in burning-velocity plots (not shown) because the resulting peak temperatures are far above the corresponding crossover values at these pressures, shown

in the upper panel of Fig. 1. Much better agreement is found for diluted conditions that lower the peak temperature to values typically found in applications, for which the reduced chemistry describes with sufficient accuracy the flame response to strain, including the critical value of the strain rate at extinction.

The intermediate and lower plots of Fig. 4 show results of diffusion flames involving a stream of air counterflowing against a stream of hydrogen diluted with nitrogen, both feed streams at $T = 300$ K, with $X_{H_2,0}$ denoting the fuel mole fraction in its feed stream. Besides intermediate panels representing the variation with strain rate of the peak temperature, the figure shows in the accompanying lower panels the associated burning rate per unit flame area $\dot{m}_{H_2}$ (mols cm^{-2} s^{-1}) obtained by integrating the fuel consumption rate across the mixing layer. In the one-step computations, the fuel consumption rate is simply 2ω, with ω given in (9), whereas in the detailed computations the evaluation accounts for the separate contributions of the five elementary reactions of the 20-step mechanism that involve H_2 molecules, namely, $H_2+O \overset{2}{\rightleftharpoons} OH+H$, $H_2+OH \overset{3}{\rightleftharpoons} H_2O+H$, $HO_2+H \overset{6}{\rightleftharpoons} H_2+O_2$, $H+H+M \overset{9}{\rightleftharpoons} H_2+M$, and $H_2 + HO_2 \rightleftharpoons H_2O_2 + H$.

It can be seen from the intermediate and lower plots that the one-step mechanism reproduces the expected decrease of peak temperature and associated increase of burning rate with increasing strain rate, until a maximum value of the strain rate A_{ext} is reached at which extinction is seen to occur. Since the computations employ a time-marching scheme, which is advanced in time until a steady solution is attained, only the upper branch of the S-shape curve of the peak temperature as a function of a Damkholer number based on the strain rate can be described. The agreement between the one-step and the detailed-chemistry computations is excellent for the largest dilution considered ($X_{H_2,0} = 0.25$), especially for $p = 50$ atm, for which the departures in the predicted peak temperatures are only about 10K and the error in the critical strain rate at extinction is only about 10%. The agreement deteriorates with decreasing dilution, as the peak temperature in the reaction region departs farther from the crossover temperature, but the general predictive capability remains satisfactory for most purposes, especially away from extinction, where transport rates of chemical intermediates are less pronounced, thereby favoring steady-state approximations [24].

To gain further insight into the effects of strain on the reduced-chemistry performance, insets showing the spatial distribution of fuel burning rate across the one-dimensional diffusion flame with $X_{H_2,0} = 0.25$ are included in the lower panels. The left inset ($p = 25$ atm) depicts the structure of a weakly strained flame, while the right inset ($p = 50$ atm) represents a nearly extinguished flame. The stagnation plane, marked with a dashed line, separates the air stream, flowing from above, from the fuel stream, with the distance from the stagnation plane scaled with the characteristic mixing-layer thickness D_T/A, where D_T is the thermal diffusivity. For the robust flame depicted on the left inset the agreement between the detailed-chemistry results and the reduced kinetics is remarkably good, indicating that at these low strain rates effects of radical transport remain limited. Near extinction, however, the flame thickness predicted by the one-step kinetics, assuming all radicals to be in steady state, is significantly smaller than that of the detailed-chemistry results. It is interesting that this nonnegligible difference in flame structure, which can be attributed to effects of preferential diffusion of H atoms in the presence of high strain rate [5], does not affect significantly the resulting peak temperature or the burning rate per unit flame area $\dot{m}_{H_2}$, so that for diluted flames the overall predictive capabilities of the reduced kinetics remain largely satisfactory even as extinction is approached.

Partially premixed fronts The one-dimensional canonical flows investigated above (i.e. steady planar deflagration and counterflow diffusion flame) are useful in characterizing premixed and nonpremixed combustion, but are not suitable for addressing partially premixed conditions, which often prevail near injectors in gas-turbine combustion chambers. In these region, combustion occurs in the form of triple and edge flames propagating along strained mixing layers at velocities (relative to the local flow) that are comparable to those of laminar premixed flames [25]. These reactive fronts play a fundamental role in the stabilization of the combustion process. There is interest, therefore, in assessing whether the one-step kinetics is able to describe sufficiently accurately the propagation of partially premixed fronts under varying levels of strain. A simple problem that serves to investigate these effects is the reactive front propagating along a mixing layer separating two opposed planar jets of fuel and oxidizer, a canonical configuration used previously in theoretical [26–28], experimental [29–31], and numerical [22, 32] studies.

The variation with strain rate of the resulting propagation velocity U when the oxidizer is air and the fuel is a mixture of H_2 and N_2 with $X_{H_2,0} = 1, 0.5, 0.25$ is shown in Fig. 6 for $p = 25$ atm and $p = 50$ atm. The flow ahead of the front is chemically frozen, so that the air mixes with the fuel to generate a mixing layer, across which the composition varies from fuel-rich to fuel-lean conditions, creating the partially premixed conditions encountered by the triple flame, which leaves behind a diffusion flame that eventually develops into the one-dimensional solution described earlier in Fig. 5. For weakly strained configurations with small values of A the mixing layer is much thicker

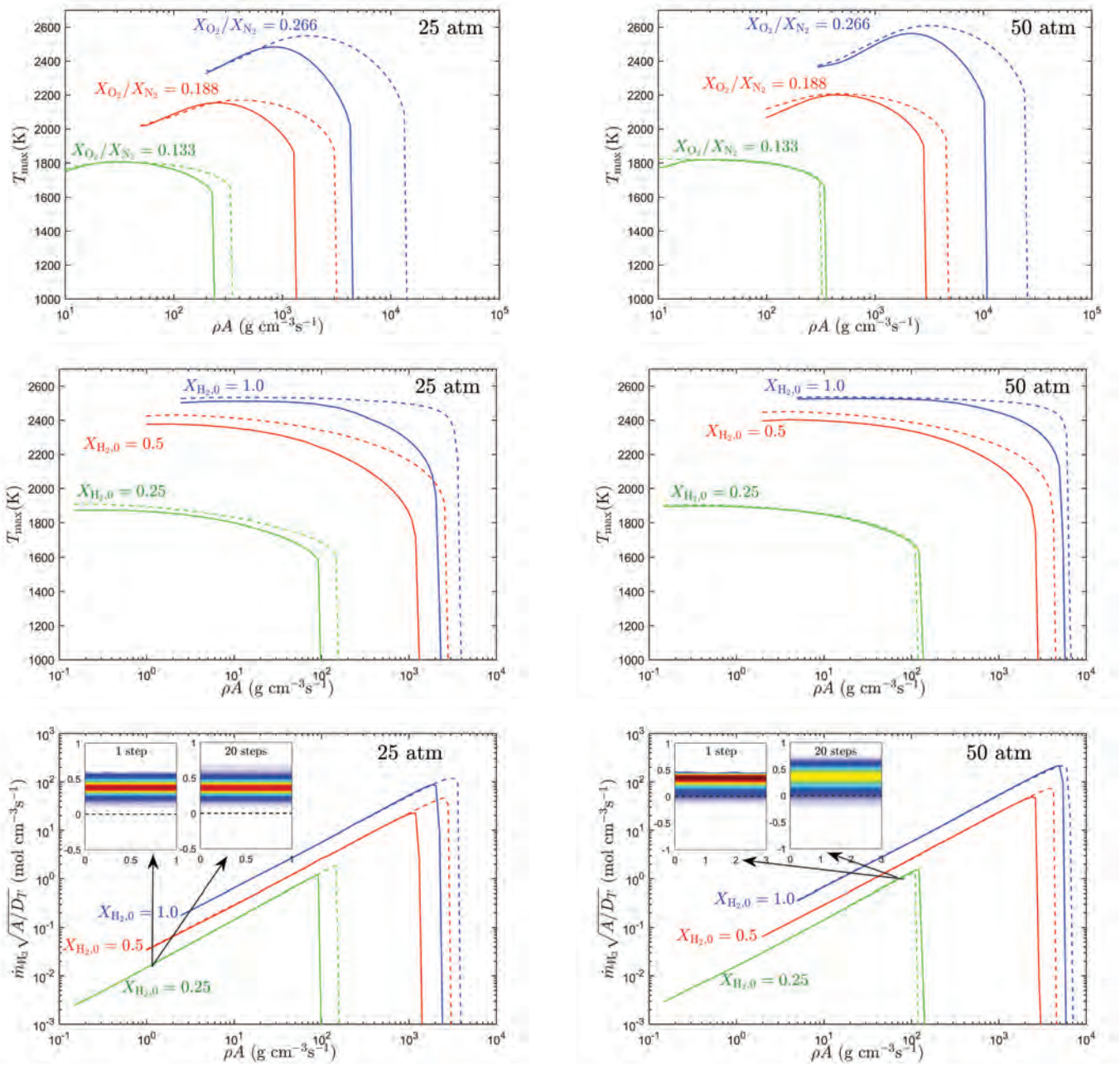

Figure 5: Results of twin premixed flames (upper plots) and diffusion flames (intermediate and lower plots) in a planar counterflow mixing layer as obtained with detailed chemistry (solid curves) and one-step reduced chemistry (dashed curves) for $p = 25$ atm and $p = 50$ atm. The upper plots give the variation with strain rate of the peak temperature in twin-premixed-flames configurations corresponding to H_2-O_2-N_2 mixtures at $T = 300$ K for three different levels of dilution X_{O_2}/X_{N_2}. The intermediate and lower plots give the variation with strain rate of the peak temperature and hydrogen burning rate for a diffusion flame formed between counterflowing streams of air and hydrogen diluted with nitrogen, with $X_{H_2,0}$ representing the hydrogen mole fraction in its feed stream. The color contours in the insets represent the local hydrogen burning rate (mols per unit volume per unit time) of a diffusion flame in a low-strain mixing layer at $p = 25$ atm (left plot) and of a diffusion flame in a high-strain mixing layer near extinction for $p = 50$ atm (right plot).

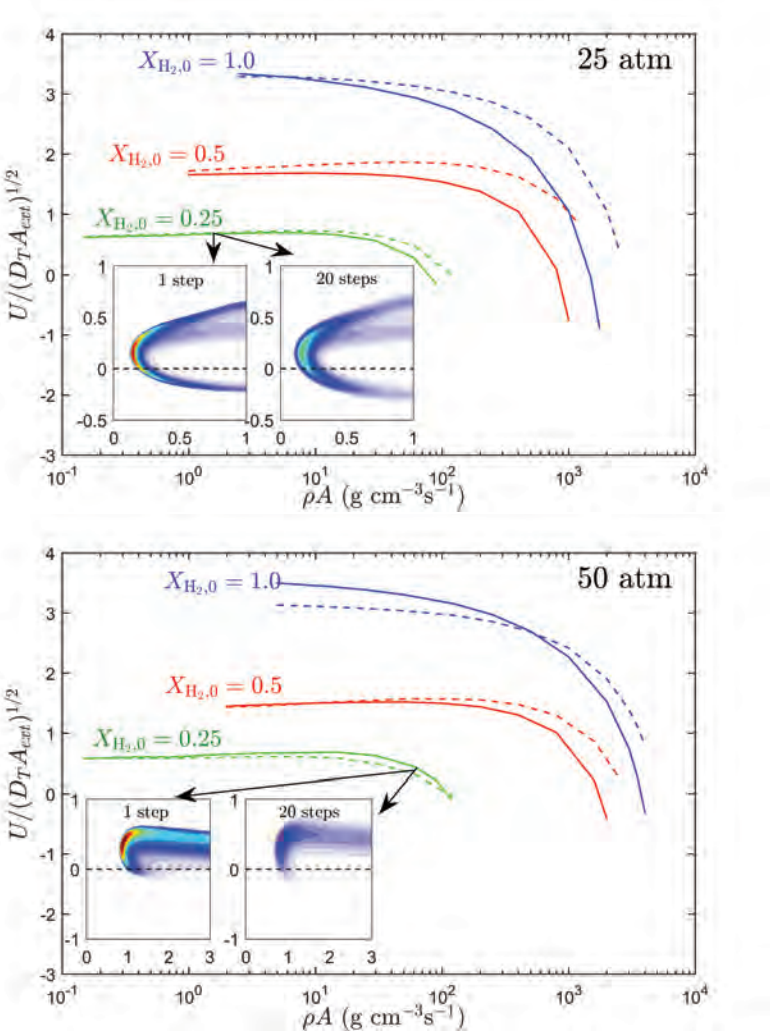

Figure 6: The variation with strain of the velocity U of a triple flame propagating along a two-dimensional mixing layer separating counterflowing streams of air and hydrogen diluted with nitrogen, with $X_{H_2,0}$ representing the hydrogen mole fraction in its feed stream. The velocity is scaled with $(D_T A_{ext})^{1/2}$, where D_T and A_{ext} represent, the thermal diffusivity and the extinction strain rate, respectively, the latter evaluated from the detailed-chemistry computations of Fig. 5. The color contours in the insets represent the local hydrogen burning rate (mols per unit volume per unit time) of an advancing front in a low-strain mixing layer at $p = 25$ atm (upper plot) and of a retreating front near extinction for $p = 50$ atm (lower plot).

than the front thickness, and a tribrachial structure emerges, including distinct lean and rich branches and a trailing diffusion flame originating from the stoichiometric point. A representative flame is shown in the inset of the upper figure, which shows contours of local fuel burning rate obtained with the detailed and reduced chemistry for the conditions of strain considered earlier in the diffusion-flame computations shown in the left inset of Fig. 5. As can be seen, although for these strain conditions reduced-chemistry fuel-consumption-rate departures are found near the triple point, where the reduced-chemistry results exhibit peak burning rates that are significantly higher than those predicted with the detailed chemistry, which spreads the reactions over larger volumes through radical diffusion. These differences, which likely arise from the high curvature of the front near the triple point, are consistent with previous numerical computations [5], which have shown how flame curvature promotes preferential diffusion of H atoms into pockets of reactants, thereby increasing overall consumption rates by spreading the chemistry over larger volumes (although locally decreasing peak reaction rates).

The propagation speed decreases for increasing strain rates, as the front loses its tribrachial structure to become an edge flame, eventually transitioning to a retreating front with negative U, which extinguishes as the strain rate A reaches the critical value A_{ext} predicted earlier in the computations of Fig. 5. The inset in the lower plot of Fig. 6 shows the structure of one of these near-extinction retreating flames. It is seen that the structure of the edge flame predicted with the one-step kinetics is quite different from that computed with detailed chemistry, in that the latter exhibits a larger thickness resulting from curvature and strain promoting preferential radical diffusion, which is necessarily absent in the reduced-chemistry model, which assumes all radicals to maintain steady state. It is of interest in connection with the predictive capability of the reduced kinetics that the local departures in flame structure illustrated in the insets do not affect significantly the resulting propagation velocity, which for this dilution is almost identical for the two chemistry models, as seen in the green curves.

In view of the curves depicted in Fig. 6, it can be concluded that the one-step kinetics provides a sufficiently accurate description with regards to the propagation speed of partially premixed fronts. The agreement is extremely good for $X_{\mathrm{H}_2,0} = 0.25$, especially at $p = 50$ atm, when the difference $T_{max} - T_c$ takes values on the order of 500 K. Despite the observed reduced accuracy at lower pressure and larger values of $X_{\mathrm{H}_2,0}$, it is remarkable that, even for undiluted fuel feed at $p = 25$ atm, when the difference $T_{max} - T_c$ is on the order of 1000 K, the one-step description still behaves reasonably well, thereby giving additional confidence on the predictive capabilities of the reduced kinetics.

1.2.2 Assessment of reduced chemical-kinetic mechanisms under unsteady conditions

Derivations of reduced chemical-kinetic mechanisms are often based on computations of steady flames [33], including steady planar deflagrations and counterflow diffusion flames, but the conditions found in LPREs are markedly unsteady, so that there is a need to test associated predictive capabilities under dynamic conditions, enabling assessments of steady-state assumptions for chemical intermediates to be performed. Our initial work to test the accuracy with which reduced chemistry describes unsteady hydrogen-air systems addressed the response of strained flamelets to acoustic excitation, with results published in [24]. The work has been extended over the last year to investigate another important canonical benchmark problem, namely, the onset and development of pulsating instabilities in fuel-rich mixtures. To that end, a one-step reduced chemical-kinetic mechanism describing near-critical hydrogen combustion, recently derived by assuming that all chemical intermediates maintain steady state [14], was used to investigate numerically the pulsating dynamics of fuel-rich hydrogen-air flames. The computations, considering pressures of up to 20 atmospheres, addressed the flame evolution for increasing values of the equivalence ratio ϕ, a relevant bifurcation parameter. Besides critical conditions associated with the Hopf bifurcation occurring at a critical value ϕ_c of ϕ, supercritical dynamics for $\phi > \phi_c$ is investigated, including the nonlinear gradual growth of the oscillation amplitude with increasing ϕ, the occurrence of a period-doubling bifurcation, and the emergence of nonlinear relaxation oscillations. Comparisons with results of numerical calculations employing detailed chemistry reveal that the one-step description is able to predict with unexpectedly good accuracy the flame dynamics, including the critical conditions at the bifurcations as well as the nonlinear dynamics encountered for $\phi > \phi_c$.

The complex pulsating dynamics of fuel-rich hydrogen-air deflagrations has been investigated numerically on the basis of one-dimensional time-dependent simulations employing detailed chemistry [34–42]. For a given pressure, the computations have revealed that the steady flame loses stability through a supercritical Hopf bifurcation as the equivalence ratio ϕ is increased beyond a critical value ϕ_c, smaller for higher pressure [39]. For values of ϕ near the instability threshold the resulting flame velocity varies harmonically in time about the steady value. The pulsations become progressively anharmonic on increasing ϕ until a second bifurcation, a period-doubling bifurcation, occurs.

Further increases of ϕ lead to the emergence of relaxation oscillations of increasing period. When radiative heat loss is accounted for, conditions are eventually reached for which flame propagation is no longer possible, with the predicted extinction limit differing in general from that obtained in steady computations [39].

Pulsating hydrogen-air flames constitute an attractive benchmark framework to test chemical-kinetic descriptions [43]. Experimentally measured instability thresholds can be compared with numerical results as a means to verify the accuracy of detailed mechanisms [40]. In addition, since derivations of reduced chemical-kinetic mechanisms are often based on computations of steady canonical flames [33], investigation of pulsating-flame dynamics provides a way to test associated predictive capabilities under dynamic conditions, enabling assessments of steady-state assumptions for chemical intermediates to be performed. For example, for hydrogen-air flames, the classical two-step reduced description [9], involving a chain-branching step $3H_2+O_2 \rightarrow 2H+2H_2O$ and a chain-breaking step $2H \rightarrow H_2$, with H atoms being the only radical out of steady state, has been shown to predict with excellent accuracy critical instability parameters associated with the Hopf bifurcation [44], confirming previous qualitative results derived on the basis of model-chemistry descriptions [45, 46].

Imposing a steady-state approximation for the H atom in the two-step description produces a one-step approximation for the chemistry [17]. The performance of the resulting approximation in predicting pulsating-flame dynamics has not been studied previously and therefore is tested here. In general, one-step approximations seem to be thought to be incapable of reproducing pulsating-flame predictions of detailed chemistry. Ad-hoc one-step approximations, such as one-step Arrhenius descriptions (none of which are addressed here), as well as corresponding rates found by introducing steady-state approximations for all intermediaries, apparently are considered likely to exhibit differences from detailed chemistry in predicting major aspects of pulsating dynamics, and the present work investigates whether this opinion is correct for the latter approach for fuel-rich hydrogen-air flames.

Comparisons of one-step and detailed-chemistry predictions For the fuel-rich conditions investigated here the overall rate of the global reaction (1) takes the simplified form (9), which has been shown to predict with great accuracy steady burning rates for atmospheric rich flames with $\phi \gtrsim 5$ [14]. Corresponding analyses of unsteady flame propagation have not been performed, that being the purpose of the present study, addressing hydrogen-air deflagrations at ambient and elevated pressures. The computations employ the radiation-free one-dimensional form of the conservation equations written in the low-Mach-number approximation [47]. For the fuel-rich conditions investigated here the specific heat of the gas mixture and the Lewis number of the different chemical species exhibit small relative changes that remain below 15% across the hydrogen-air flame. For this reason, the computations presented below assume a constant specific heat, selected to provide the correct value of T_a, and a Fickian diffusion model with constant Lewis numbers, evaluated from the mixture-average diffusion coefficients at equilibrium.

The numerical integration employs a numerical code based in the Lagrange-Galerkin Finite Element method, developed for transient combustion applications [48]. The code features second-order convergence in time and third-order convergence in space in the L^2-norm for sufficiently smooth solutions. The numerical method employs a local anisotropic h-adaptive algorithm to refine around the flame location, with the minimum length of the elements being $\Delta x = 0.005$ mm and the maximum length $\Delta x = 0.5$ mm. The transient one-dimensional equations were integrated numerically, marching forward in time with a time step $\Delta t = 5 \times 10^{-4}$ ms, in a large spatial domain ranging from $x = -2$ mm to $x = 10$ mm. Tests were run to guarantee that the results were independent of the time step and grid and domain sizes. The velocity at the upstream boundary U_u, where the density is ρ_u, was adjusted in the calculation to maintain the flame within the computational domain while applying an outflow boundary condition at the downstream boundary, where the velocity is U_d and the density is ρ_d. The instantaneous flame speed is evaluated using the expression $U_L = (U_d - U_u)\rho_d/(\rho_u - \rho_d)$, which is the natural correct definition in the case of steady-flame propagation (other definitions, based for example on tracking the fluid particle with the highest heat-release rate, were checked to give fundamentally equivalent results). The value of ϕ was increased by a small increment $\Delta\phi = 0.01$ in subsequent integrations that were extended in time until the solution was seen to reach a permanent state (steady, periodic, or chaotic), with the final solution for a given ϕ used as initial condition in the following integration for $\phi + \Delta\phi$.

Unsteady flame behavior The resulting transient evolution of the flame speed is shown in Fig. 7 for a hydrogen-air mixture at pressure $p = 10$ atm. Representative sample results corresponding to the detailed San Diego mechanism [19] are shown in the top plot, to be discussed first. For stable flames corresponding to values of $\phi < \phi_c$, the numerical solution evolves rapidly to recover the steady solution, as shown for $\phi = 5.1$ in Fig. 7; to illustrate the stabilization

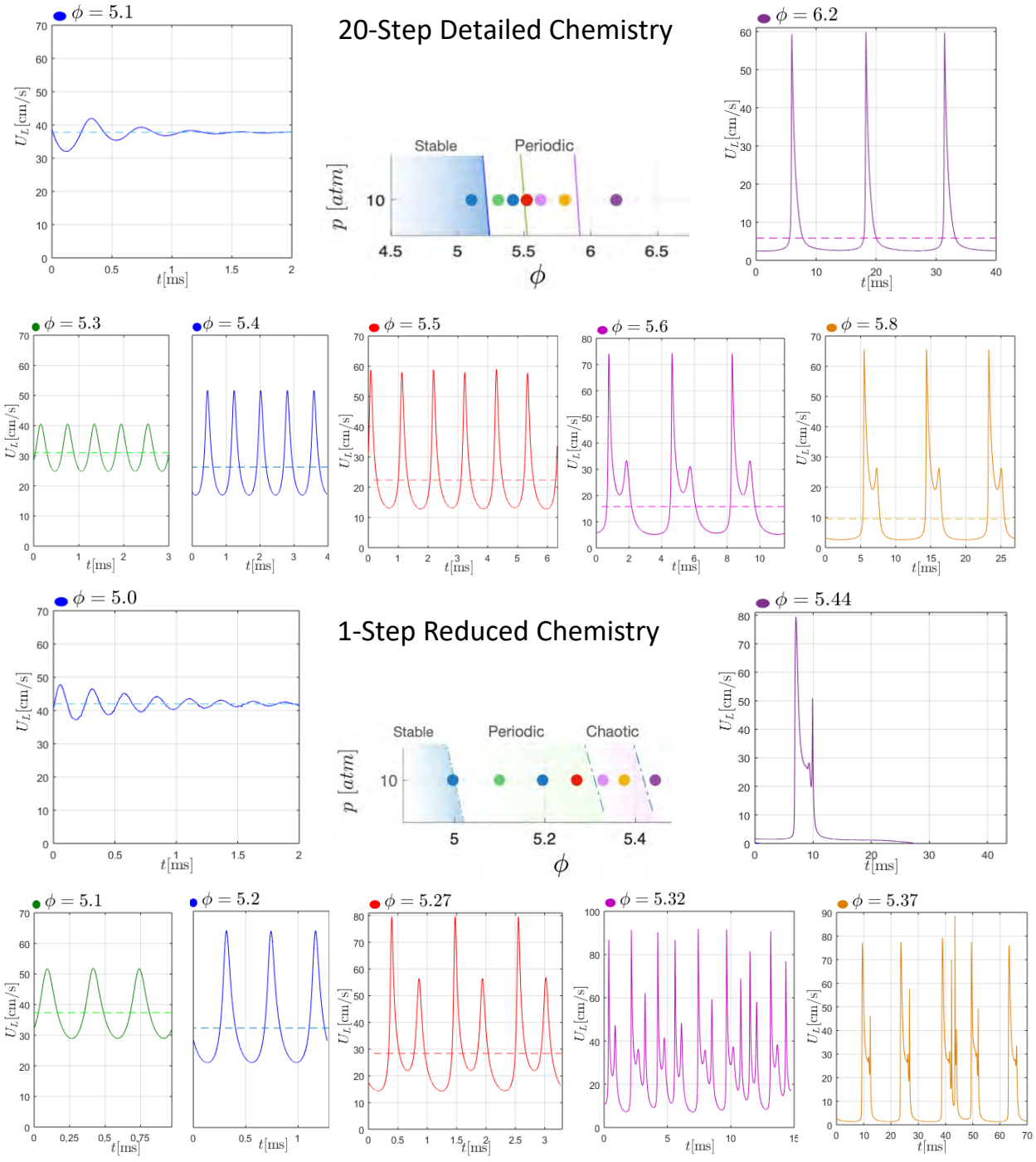

Figure 7: Time-dependent variation of the flame propagation velocity corresponding to a hydrogen-air mixture at $p = 10$ atm as obtained from numerical integrations with detailed chemistry (upper plots) and one-step reduced chemistry (lower plots) for representative values of the equivalence ratio ϕ.

process, this specific computation was initiated using an oscillating flame as initial condition. Pulsating flames arise for $\phi > \phi_c \simeq 5.26$, with associated oscillations, harmonic for $\phi = 5.3$, becoming increasingly nonlinear for $\phi = 5.4$. A second bifurcation at $\phi \simeq 5.5$ leads to flames with double-period oscillations, visible in the velocity evolution shown in the figure. Further increases of ϕ result in larger periods, eventually leading to relaxation oscillations. In the absence of heat losses, no chemical-kinetic extinction occurs, so these relaxation oscillations persist for larger values of the equivalence ratio, with the low-temperature H_2O_2 chemistry playing an increasingly important role in this nonlinear regime. At lower pressures and higher equivalence ratios the relaxation oscillations tend to become chaotic.

The results obtained with the explicit one-step description using the rate parameters of the San Diego mechanism [19] to evaluate (9) are shown in the bottom plot of Fig. 7. The reduced chemistry is seen to reproduce accurately the behavior near the bifurcation. The corresponding values of the instability parameters exhibit only small quantitative departures from the detailed-chemistry results; the critical equivalence ratio at the onset of the pulsating instability is found to be $\phi_c \simeq 5.02$ instead of 5.26, while double-period oscillations emerge for $\phi = 5.25$ instead of 5.5. Differences in ϕ_c remain about 0.2 over the entire range of pressures investigated here, including pressures of up to 20 atm, of interest in typical engine and gas-turbine applications. The subsequent evolution for increasing $\phi > \phi_c$ involves in this 10-atmosphere case a cascade of period-doubling bifurcations, leading to chaotic behavior, which eventually takes the form of chaotic relaxation oscillations, in contrast to the apparent absence of chaos with the detailed chemistry at this condition. To check the chaotic nature of the reduced-chemistry solution, numerical tests were performed using different grid spacing and different time steps. While the periodic solutions arising for $\phi \leq 5.3$ were found to be largely independent of these details of the computation, for larger values of ϕ the solution was always seen to evolve into chaotic oscillations.

Since the one-step chemistry contains a chemical-kinetic limit associated with the crossover temperature, flame extinction is observed when the equivalence ratio is further increased to values large enough for the flame peak temperature to fall below crossover during the prolonged low-velocity stages. A typical extinction event, occurring for $\phi = 5.44$, is illustrated in the bottom plot of Fig. 7. This extinction limit, of course, does not arise with detailed chemistry because it retains a low-temperature path, although if heat loss were included then the increasing length of the low-velocity period would lead to extinction.

To further quantify the performance of the reduced chemistry, Fig. 2 displays the detailed behavior of the solution near the onset of instability for a hydrogen-air flame at $p = 10$ atm. The plot of maximum and minimum propagation velocity exhibits the expected supercritical pitchfork character of the bifurcation. The comparison of the results of the two chemistry models clearly illustrates the predictive capability of the one-step chemistry. Except for the exact value of ϕ_c, which differs by about 0.2, the similarity of the results, including the growth rate of the oscillation amplitude with increasing equivalence ratios, is evident. The same type of agreement is found in connection with the resulting oscillation frequency, also shown in Fig. 2, where the dashed portion of the curves, corresponding to steady flames, is inferred from the period of the decaying oscillations encountered during the transient computations, which can be observed in the plots for $\phi = 5.1$ (detailed chemistry) and $\phi = 5.0$ (reduced chemistry) in Fig. 7. The principal difference is that the bifurcation occurs at lower equivalence ratios with one-step chemistry, as may be expected from the reduced degrees of freedom imposed by the steady-state approximations.

The H-atom steady state The unexpected degree of success of the one-step predictions suggests that the main approximation underlying the derivation of the overall hydrogen-oxidation rate (9), namely, that all radicals maintain steady state, holds true as the flame bifurcates to an oscillatory state. For most combustion practitioners, this is particularly surprising in the case of H atoms, which are generally thought to remain out of steady state, its transport rate being comparable to its production and consumption rates. If H atoms were in fact out of steady state, then the numerical computation of the oscillating flame would require a minimum of two overall steps [9], that being the description utilized in the previous stability analysis of Gubernov et al. [44], but the present results clearly indicate that that is not necessary, in that an explicit, one-step mechanism suffices to describe the main aspects of the solution.

To further test this conclusion, the right-hand-side plot of Fig. 8 represents the rates of H-atom production $\dot{m}_{\mathrm{H}_P} > 0$ and consumption $\dot{m}_{\mathrm{H}_C} < 0$ across the flame at $p = 10$ atm, with the sum $\dot{m}_{\mathrm{H}_P} + \dot{m}_{\mathrm{H}_C}$ corresponding to the radical transport rate. Besides a steady flame for $\phi = 5.2$ (A) the figure includes two snapshots of the unsteady results for an oscillatory flame with $\phi = 5.4$, with conditions B/C corresponding to the instant of minimum/maximum propagation velocity. As can be seen, for all three conditions explored in the figure, H-atom production and consumption maintain an almost exact balance all across the flame, while the transport rate remains everywhere significantly smaller. The fact that the steady state of H atoms prevails beyond the bifurcation is an important quantitative finding. In view

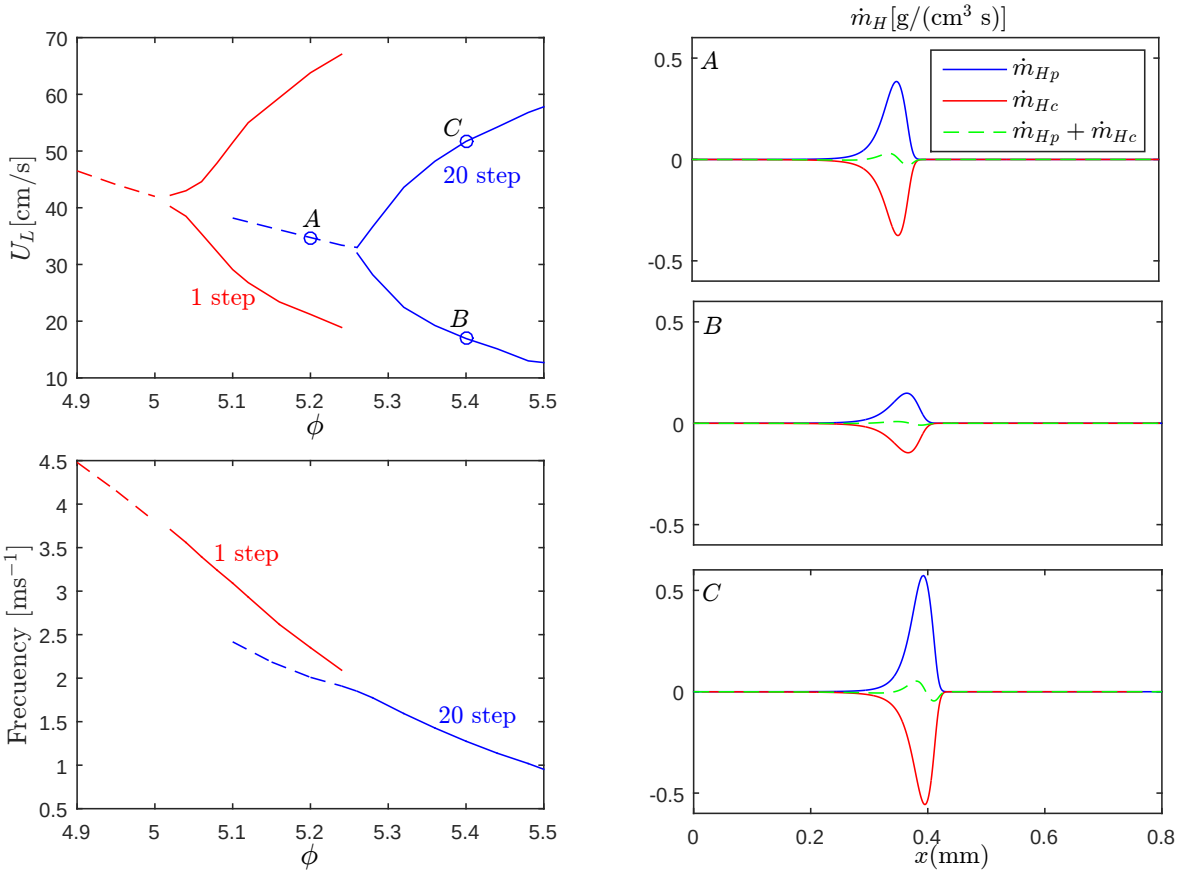

Figure 8: The flame velocity and oscillation frequency of the solution near the Hopf bifurcation for a hydrogen-air mixture at $p = 10$ atm as described with detailed chemistry (blue curves) and one-step reduced chemistry (red curves). The right-hand-side plot shows H-atom production, consumption, and transport rates across the flame for the three conditions identified with dots on the flame-velocity plot (steady flame with $\phi = 5.2$ (A), oscillating flame with $\phi = 5.4$ at instants of minimum velocity (B) and maximum velocity (C).

of this results, it can be expected that the one-step mechanism, previously tested for steady flames [14, 17, 18], can also be used to describe unsteady flame dynamics, provided that the associated characteristic times remain sufficiently larger than the typical chemical times, that being the case for the oscillatory flames investigated here.

The bifurcation diagram The values of ϕ_c determined for pressures in the range 1 atm $\leq p \leq$ 20 atm are represented in Fig. 9 with thick curves. There is seen to be reasonably close agreement between the predictions obtained with detailed chemistry (solid curve) and one-step reduced chemistry (dashed curve). The observed decrease of ϕ_c with increasing pressure is consistent with that obtained in previous computations [39]. It is of interest that the stability boundary lies parallel to the chemical-kinetic limit $T_a = T_c$ corresponding to crossover, represented by a thin dashed curve in the plot. The fact that the difference between ϕ_c and the chemical-kinetic flammability limit is nearly independent of the pressure seems to indicate that the instability occurs when the peak temperature exceeds the crossover temperature by a fixed critical amount. These considerations might help guide future analytical work aimed at extending Sivashinsky's analysis [49], corresponding to Arrhenius chemistry, to the non-Arrhenius rate expression (9).

The plot also shows the regions of existence of single-period oscillations, double-period oscillations, and relaxation oscillations, with separating boundaries corresponding to the detailed-chemistry predictions. It can be seen that these boundaries tend to merge for $p \lesssim 5$ atm. For these reduced pressures, the numerical integrations with both detailed and reduced chemistry reveal that the first bifurcation is followed by a rapid cascade of double-period bifurcations that lead to the establishment of chaotic relaxation oscillations, qualitatively similar to those displayed in the reduced-chemistry results for $\phi = 5.37$ in Fig. 7.

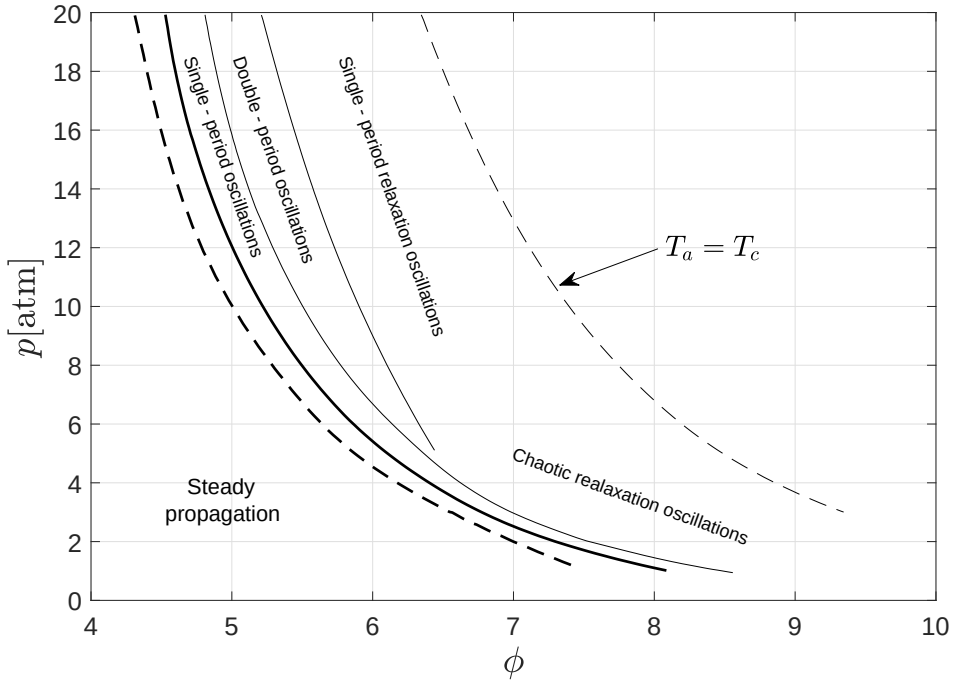

Figure 9: Parametric dependence of bifurcation boundaries.

1.2.3 Propagation of partially premixed fronts along mixing layers

Although in most LPREs combustion occurs predominantly in the form of non-premixed flames, there exist regions in the combustion chamber where combustion occurs instead in a partially premixed mode. That is especially true near the injectors, where we find edge flames moving along thin mixing layers that are strained by the turbulent flow. These flames, propagating relative to the local flow at velocities that are comparable to those of laminar premixed flames, play a fundamental role in the stabilization of the combustion process in LPREs, where the flame often appears

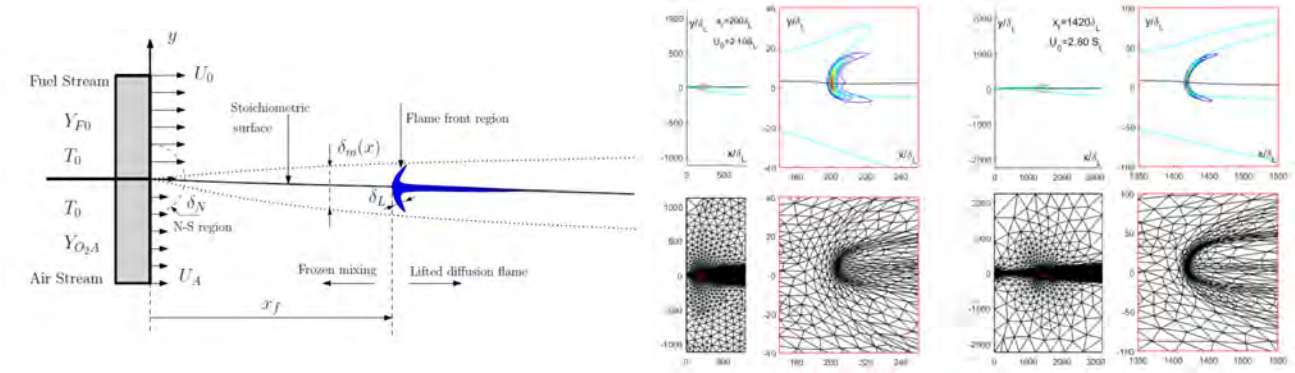

Figure 10: The flow configuration employed in the triple-flame computations (left plot) and sample results corresponding to two injection velocities (right plot).

lifted downstream from the fuel injection plane. While there exists substantial knowledge of many aspects related to the structure and propagation of edge flames [25], more work is needed to clarify their dynamics, including their propagation speed and their transient flame response to acoustic oscillations.

The work has focused on the quantification of the propagation speed U_0, which is known to be larger than that of the planar stoichiometric flame S_L as a result of flow redirection upstream from the flame [50]. This effect was quantified using the porous-wall configuration indicated on the right-hand side of Fig. 10. The numerical solution provides the flame location x_f as a function propagation velocity U_0, with the value of x_f diverging as the maximum propagation velocity is achieved. Previous numerical integrations for methane-air systems [51], shown as dots in Fig. 10, determined a value $U_0 = 3.2S_L$. However, our results indicate that the maximum value exceeds $U_0 = 4S_L$. As can be seen in the figure, the computations need to be extended to larger domains, since the resulting curve $x_f - U_0$ is still far from reaching the expected vertical asymptote denoting the maximum propagation velocity. The ongoing computations will provide, for the first time, an accurate quantification of the velocity-augmentation factor, probably exceeding $U_0/S_L = 4.2$.

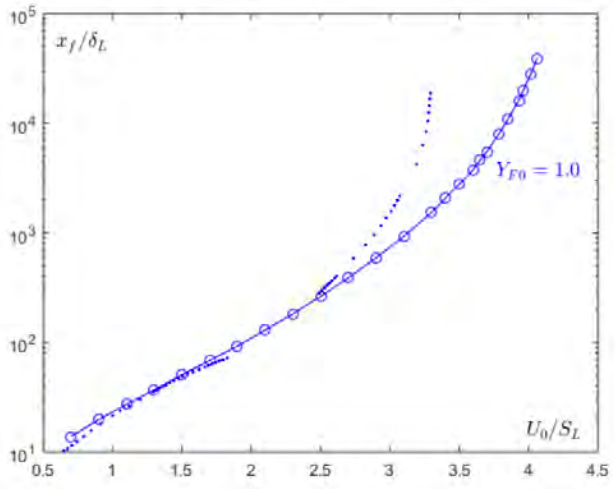

Figure 11: The variation of the flame location (scaled with the flame thickness) with the injection velocity (scaled with the planar deflagration velocity S_L).

1.2.4 Conclusions

Replacing the available detailed mechanisms of twenty or more steps by a one-step mechanism can be quite beneficial in computational investigations of hydrogen LPREs, provided that the one-step mechanism delivers sufficient accuracy for the chemical kinetics. It may be seen from the results reported herein that, by restricting attention to the combustor pressures, temperatures, and mixture compositions commonly encountered in practical systems, not only premixed laminar flame temperatures and burning velocities, but also peak temperatures in strained twin-flame configurations, counterflow diffusion-flame peak temperatures, burning rates, and extinction conditions, and rates of advancement or retreat of partially premixed triple or edge flames, all are predicted with errors at most of the order of ten percent, by the one-step mechanism derived in the present work. Also, the investigation of pulsating flames demonstrates that the predictive capabilities of the one-step description extend to dynamic conditions, suggesting that local accumulation rates of chemical intermediates remain small enough for the associated steady states to continue to hold during unsteady flame propagation. This mechanism therefore is likely to be useful in future computational and theoretical investigations. Exploring the applicability of the ideas developed here to hydrocarbon combustion at high pressure warrants future investigation.

1.3 Dissemination activities

Results of this project pertaining to the performance of reduced kinetics under unsteady conditions were presented at the 12th U.S. National Combustion Meeting. The developments described above have resulted so far in two publications:

- A. L. Sánchez, J. Carpio, F. A. Williams, Unexpected performance of systematically derived one-step chemistry in describing rich hydrogen-air pulsating flames, *Combust. Flame*, **241** 112068 (2022)
- J. Carpio, B. Li, D. Fernández-Galisteo, A. L. Sánchez, F. A. Williams, Systematically derived one-step kinetics for hydrogen-air gas-turbine combustion, *Combust. Flame*, under review (2022)

2 Impacts

2.1 Development of the principal discipline of the project

The present project has addressed finite-rate kinetics in connection with its role in the complex acoustic-flow interactions leading to the onset and development of LPRE instabilities, with specific attention given to the development of appropriate chemistry models that can facilitate numerical computation of high-pressure reactive systems with different levels of complexity. A simplified chemistry model has been developed and tested thoroughly for application in numerical and analytical studies of LPRE combustion. The computations presented in this project indicate that, for high-pressure combustion in hydrogen systems, all chemical intermediates follow a steady state approximation with reasonably good accuracy, so that their transport rate can be neglected in describing the reactive process. As a result, the combustion process, which fundamentally involves 20 elementary reactions among 8 reactive species, can be effectively represented with the single overall step $2H_2+O_2 \rightarrow 2H_2O$, whose rate is systematically derived from the detailed-chemistry description, resulting in a non-Arrhenius explicit expression involving the rate parameters of a few elementary reactions. The mechanism has been found to describe with reasonably good accuracy many aspects of the reactive process, including flame structures and propagation velocities, response to strain, and partially premixed fronts. Predictive capabilities in connection with unsteady phenomena have been tested by using the pulsating dynamics of fuel-rich hydrogen-air flames as benchmark, complementing previous specific work focused on acoustic-pressure response. Comparisons with results of numerical calculations employing detailed chemistry reveal that the one-step description is able to predict with unexpectedly good accuracy the flame dynamics, including the critical conditions at the bifurcations as well as the supercritical nonlinear dynamics. These findings suggest that the one-step mechanism proposed here constitutes an effective tool for describing high-pressure hydrogen combustion. Besides its applicability in relation to LPREs, the mechanism can be also used in numerical computations of hydrogen-fueled gas turbines, of primary interest in foreseeable carbon-free energy-production scenarios. Future work should extend the ideas developed here to explore the applicability of the steady-state approximation for chemical intermediates in connection with other fuels or fuel mixtures.

2.2 Other disciplines

Nothing to Report

2.3 Describe the impact in this reporting period on the development of human resources

One graduate student (Brandon Li) has been working on the project. The results of high-pressure combustion will be part of his dissertation. In his future PhD work he will investigate extensions of the ideas presented above to other fuels or mixtures of fuels.

2.4 Describe the impact on teaching and educational experiences

Nothing to Report

2.5 Describe the impact in this reporting period on physical, institutional, and information resources that form infrastructure

Nothing to Report

2.6 Impact on society beyond science and technology

Nothing to Report

3 Changes

Nothing to Report

4 Technical updates

Nothing to Report

References

[1] JF Griffiths. Reduced kinetic models and their application to practical combustion systems. *Progress in energy and combustion science*, 21(1):25–107, 1995.

[2] Tianfeng Lu and Chung K Law. Toward accommodating realistic fuel chemistry in large-scale computations. *Progress in Energy and Combustion Science*, 35(2):192–215, 2009.

[3] Forman A Williams. *Combustion Theory*. Benjamin Cummings, 1985.

[4] M R Bothien, A Ciani, J P Wood, and Fruechtel G. Toward decarbonized power generation with gas turbines by using sequential combustion for burning hydrogen. *J. Eng. Gas Turbines Power*, 141:121013, 2019.

[5] M Reith, A Gruber, F A Williams, and J H Chen. Enhanced burning rates in hydrogen-enriched turbulent premixed flames by diffusion of molecular and atomic hydrogen. *Combust. Flame*, 239:111740, 2022.

[6] Terence P Coffee, Anthony J Kotlar, and Martin S Miller. The overall reaction concept in premixed, laminar, steady-state flames. I. Stoichiometries. *Combust. Flame*, 54:155–169, 1983.

[7] Vadim N Gamezo, Takanobu Ogawa, and Elaine S Oran. Numerical simulations of flame propagation and DDT in obstructed channels filled with hydrogen–air mixture. *Proc. Combust. Inst.*, 31:2463–2471, 2007.

[8] Bing Wang, Wei Wei, Suna Ma, and Gao Wei. Construction of one-step H_2/O_2 reaction mechanism for predicting ignition and its application in simulation of supersonic combustion. *Int. J. Hydrog. Energy*, 41:19191–19206, 2016.

[9] Antonio L Sánchez and Forman A Williams. Recent advances in understanding of flammability characteristics of hydrogen. *Prog. Energy Combust. Sci.*, 41:1–55, 2014.

[10] Fabian Mauss, Norbert Peters, Bernd Rogg, and FA Williams. Reduced kinetic mechanisms for premixed hydrogen flames. In *Reduced kinetic mechanisms for applications in combustion systems*, pages 29–43. Springer, 1993.

[11] Pierre Boivin, Antonio L Sánchez, and Forman A Williams. Four-step and three-step systematically reduced chemistry for wide-range H_2–air combustion problems. *Combust. Flame*, 160:76–82, 2013.

[12] Antonio L Sánchez, Amable Liñán, and Forman A Williams. Chain-branching explosions in mixing layers. *SIAM J. Appl. Math.*, 59:1335–1355, 1999.

[13] K Gkagkas and RP Lindstedt. The impact of reduced chemistry on auto-ignition of H_2 in turbulent flows. *Combust. Th. Model.*, 13:607–643, 2009.

[14] Daniel Fernández-Galisteo, Adam Weiss, Antonio L Sánchez, and Forman A Williams. A one-step reduced mechanism for near-limit hydrogen combustion with general stoichiometry. *Combust. Flame*, 208:1–4, 2019.

[15] Antonio L Sánchez and Forman A Williams. Corrigendum to "recent advances in understanding of flammability characteristics of hydrogen" [Prog. Energy Combust. Sci. 41 (2014) 1–55]. *Prog. Energy Combust. Sci.*, 54:93–94, 2016.

[16] Antonio L Sánchez, Jaime Carpio, and Forman A Williams. Unexpected performance of systematically derived one-step chemistry in describing rich hydrogen-air pulsating flames. *Combust. Flame*, 241:112068, 2022.

[17] Daniel Fernández-Galisteo, AL Sánchez, A Liñán, and FA Williams. One-step reduced kinetics for lean hydrogen–air deflagration. *Combust. Flame*, 156:985–996, 2009.

[18] Daniel Fernández-Galisteo, AL Sánchez, A Liñán, and FA Williams. The hydrogen–air burning rate near the lean flammability limit. *Combust. Th. Model.*, 13:741–761, 2009.

[19] The San Diego Mechanism: Chemical-Kinetic Mechanisms for Combustion Applications. https://web.eng.ucsd.edu/mae/groups/combustion/mechanism.html, 2016. Version: 2016-12-14.

[20] Robert J Kee, Graham Dixon-Lewis, Jürgen Warnatz, Michael E Coltrin, and James A Miller. A Fortran computer code package for the evaluation of gas-phase multicomponent transport properties. Technical Report SAND86-8246, Sandia Labs., Livermore, CA (United States), 1986.

[21] Phillip H Paul. DRFM: A new package for the evaluation of gas-phase transport properties. Technical report, Sandia Labs., Livermore, CA (United States), 1997.

[22] Jaime Carpio, Prabakaran Rajamanickam, Antonio L Sánchez, and Forman A Williams. Near-limit H_2-O_2-N_2 combustion in nonpremixed counterflow mixing layers. *Combust. Flame*, 216:426–438, 2020.

[23] Paul A Libby, Amable Liñán, and Forman A Williams. Strained premixed laminar flames with nonunity lewis numbers. *Combust. Sci. Technol.*, 34:257–293, 1983.

[24] Adam D Weiss, Antonio L Sánchez, and Forman A Williams. Accuracies of reduced mechanisms for predicting acoustic combustion instabilities. *Combust. Flame*, 209:405–407, 2019.

[25] Amable Linán, Marcos Vera, and Antonio L Sánchez. Ignition, liftoff, and extinction of gaseous diffusion flames. *Annu. Rev. Fluid Mech.*, 47:293–314, 2015.

[26] J Daou and A Liñán. The role of unequal diffusivities in ignition and extinction fronts in strained mixing layers. *Combust. Theory Model.*, 2:449–477, 1998.

[27] J Daou and A Liñán. Triple flames in mixing layers with nonunity Lewis numbers. *Symp. (Int.) Combust.*, 27:667–674, 1998.

[28] Prabakaran Rajamanickam, Wilfried Coenen, Antonio L Sánchez, and Forman A Williams. Influences of stoichiometry on steadily propagating triple flames in counterflows. *Proc. Combust. Inst.*, 37:1971–1977, 2019.

[29] Min Suk Cha and Paul D Ronney. Propagation rates of nonpremixed edge flames. *Combust. Flame*, 146:312–328, 2006.

[30] Hang Song, Philip Wang, Richard S Boles, David Matinyan, Hatsachai Prahanphap, Jesse Piotrowicz, and Paul D Ronney. Effects of mixture fraction on edge-flame propagation speeds. *Proc. Combust. Inst.*, 36:1403–1409, 2017.

[31] Zhenghong Zhou, Siena S Applebaum, and Paul D Ronney. Effect of stoichiometric mixture fraction on nonpremixed H_2-O_2-N_2 edge-flames. *Proc. Combust. Inst.*, 37:1989–1996, 2019.

[32] Faisal Al-Malki and Paul Ronney. The combined effects of chemical reaction order and stoichiometry on nonpremixed edge flames. *Combust. Theory Model.*, 25:1195–1210, 2021.

[33] Norbert Peters and Bernd Rogg. *Reduced kinetic mechanisms for applications in combustion systems*, volume 15. Springer Science & Business Media, 2008.

[34] K Kailasanath, K Ganguly, and G Patnaik. Dynamics of flames near the rich-flammability limit of hydrogen-air mixtures. *Progress in Astronautics and Aeronautics*, 151:247–247, 1993.

[35] Longting He and Paul Clavin. Premixed hydrogen-oxygen flames. part I: Flame structure near the flammability limits. *Combust. Flame*, 93:391–407, 1993.

[36] Longting He and Paul Clavin. Premixed hydrogen-oxygen flames. part II: Quasi-isobaric ignition near the flammability limits. *Combust. Flame*, 93:408–420, 1993.

[37] G Goyal, U Maas, and J Warnatz. Simulation of the behavior of rich hydrogen-air flames near the flammability limit. *Combust. Sci. Technol.*, 105:183–193, 1995.

[38] EW Christiansen, CJ Sung, and CK Law. Pulsating instability in near-limit propagation of rich hydrogen/air flames. *Symp. (Int.) Combust.*, 27:555–562, 1998.

[39] EW Christiansen, CK Law, and CJ Sung. Steady and pulsating propagation and extinction of rich hydrogen/air flames at elevated pressures. *Combust. Flame*, 124:35–49, 2001.

[40] AI Korsakova, VV Gubernov, AV Kolobov, V Bykov, and U Maas. Stability of rich laminar hydrogen-air flames in a model with detailed transport and kinetic mechanisms. *Combust. Flame*, 163:478–486, 2016.

[41] AI Korsakova, VV Gubernov, V Bykov, and U Maas. The effect of soret diffusion on stability of rich premixed hydrogen–air flames. *Int. J. Hydrog. Energy*, 41:17670–17675, 2016.

[42] VV Gubernov, V Bykov, and U Maas. The effect of dilution on the diffusive-thermal instability of the rich premixed hydrogen deflagration. *Int. J. Hydrog. Energy*, 44:11153–11160, 2019.

[43] Viatcheslav Bykov, Sudhi Shashidharan, Etele Berszany, Vladimir Gubernov, and Ulrich Maas. Model reduction of rich premixed hydrogen/air oscillatory flames by global quasi-linearization (gql). *Combustion Science and Technology*, pages 1–18, 2021.

[44] VV Gubernov, AV Kolobov, V Bykov, and U Maas. Investigation of rich hydrogen–air deflagrations in models with detailed and reduced kinetic mechanisms. *Combust. Flame*, 168:32–38, 2016.

[45] Vladimir V Gubernov, Andrei V Kolobov, Andrei A Polezhaev, and Harvinder S Sidhu. Stability of combustion waves in the zeldovich–liñán model. *Combust. Flame*, 159:1185–1196, 2012.

[46] Vladimir V Gubernov, Andrei V Kolobov, Andrei A Polezhaev, and Harvinder S Sidhu. Analysing the stability of premixed rich hydrogen–air flame with the use of two-step models. *Combust. Flame*, 160:1060–1069, 2013.

[47] Mitchell D Smooke. The computation of laminar flames. *Proc. Combust. Inst.*, 34:65–98, 2013.

[48] Jaime Carpio, Juan Luis Prieto, and Marcos Vera. A local anisotropic adaptive algorithm for the solution of low-Mach transient combustion problems. *J. Comput. Phys.*, 306:19–42, 2016.

[49] GI Sivashinsky. Diffusional-thermal theory of cellular flames. *Combust. Sci. Technol.*, 15:137–145, 1977.

[50] GR Ruetsch, L Vervisch, and A Liñán. Effects of heat release on triple flames. *Physics of Fluids*, 7(6):1447–1454, 1995.

[51] Eduardo Fernández-Tarrazo, Marcos Vera, and Amable Liñán. Liftoff and blowoff of a diffusion flame between parallel streams of fuel and air. *Combustion and flame*, 144(1-2):261–276, 2006.